Sound propagation from a ridge wind turbine across a valley

By Timothy Van Renterghem*

Ghent University, Department of Information Technology, iGent tower, Technologiepark 15, 9052 Zwijnaarde, Belgium

Keywords: outdoor sound propagation; wind turbine; undulating terrain; Parabolic Equation method

Summary

Sound propagation outdoors can be strongly affected by ground topography. The existence of hills and valleys between a source and receiver can lead to the shielding or focussing of sound waves. Such effects can result in significant variations in received sound levels. In addition, wind speed and air temperature gradients in the atmospheric boundary layer also play an important role. All of the foregoing factors can become especially important for the case of wind turbines located on a ridge overlooking a valley. Ridges are often selected for wind turbines in order to increase their energy capture potential through the wind speed up effects often experienced in such locations. In this paper, a hybrid calculation method is presented to model such a case, relying on an analytical solution for sound diffraction around an impedance cylinder and the conformal mapping (CM) Green's Function Parabolic Equation (GFPE) technique. The various aspects of the model have been successfully validated against alternative prediction methods. Example calculations with this hybrid analytical-CM-GFPE model show the complex sound pressure level distribution across the valley and the effect of valley ground type. The proposed method has the potential to include the effect of refraction through the inclusion of complex wind and temperature fields, although this aspect has been highly simplified in the current simulations.

*Author for correspondence (timothy.van.renterghem@intec.ugent.be).

1. Introduction

In order to fulfil the renewable energy targets that have been set in many countries, the number of wind turbines is expected to increase significantly in the near future. Among the different environmental impacts associated with wind turbines (such as landscape and visual impact, shadow flicker, impact on wildlife, electromagnetic interference and climate change [1]), noise issues remain the key environmental factor controlling the extent of a wind farm's development [2]. Even at low A-weighted sound pressure levels, there is a substantial negative perception towards wind turbine noise [3, 4, 5, 6, 7, 8]. Therefore, noise impact assessments are commonly required during the planning phase.

Positioning wind turbines on ridges can potentially intensify momentum extraction from the wind flow [9], caused by the so-called wind-speed up effect [10, 11, 12]. Parameters of relevance include hill shape, the terrain upwind of the hill, atmospheric stability, and whether or not the hill is forested [9, 10, 11, 12].

However, there is little research, to the author's knowledge, regarding sound propagation from a ridge mounted wind turbine to receptor locations across an adjacent valley, although the measurement based studies of Evans and Cooper [13] have highlighted the importance of topography, including valleys, for wind turbine noise propagation. Established knowledge from other types of environmental noise sources cannot be easily transferred to the present case due to the unique positioning of the source high above a ridge. Physical phenomena that could be relevant to the present case include amplification of sound due to the valley (potentially mediated or intensified by the valley shape and its acoustic ground impedance), partial shielding by the ridge, and atmospheric refraction and turbulent scattering of sound waves due to the complex flow fields that are expected in such a geometry. Both the hilly topography and the presence of a turbine will add to the complexity of the flow. In this work, some of these aspects are studied by means of numerical sound propagation modelling.

Study of the foregoing expected sound propagation effects demand an advanced outdoor sound propagation technique. However, consideration additionally needs to be given to the computational cost, and therefore also the practical applicability of any such advanced techniques. Meta-analysis of (perception) studies with regards to wind turbine noise annoyance in Ref. [14] state that below 35 dBA negative effects are generally not found. Logically, the latter defines the distance of concern. For large horizontal axis wind turbines, with total source power levels easily exceeding 100 dBA when operating near their maximum power production, a propagation distance of minimum 1 km from the source should be attained. Knowing that wind turbine noise emission spectra typically show a maximum near the octave band of 1 kHz [15, 16], and given that sufficiently detailed wave propagation techniques need sub-wavelength discretisation, the numerical problem becomes challenging regarding spatio-temporal discretisation.

An interesting candidate is the Parabolic Equation (PE) method (see e.g. Refs [17, 18]). The simplification to one-way sound propagation allows efficient solving of the governing sound propagation equations. In addition, a refracting atmosphere can be accounted for in detail. For many cases involving long-distance sound propagation, reasonably accurate predictions can be made with this methodology. Of specific interest is the Green's Function Parabolic Equation (GFPE) method [19, 20], as this allows forward stepping at multiples of the wavelength in contrast to the sub-wavelength step spacing of most other advanced techniques.

The GFPE, however, cannot be readily used to model sound propagation from a ridge mounted wind turbine. The inclusion of undulating terrain will be discussed in this work, and a number of specific problems will be dealt with. Focus is on accurately accounting for the effect of terrain undulation in the case of a source positioned high above a ridge. In addition, some example calculations are provided to show the potential of the proposed model.

In the present paper, the specific wind and temperature fields near a ridge wind turbine are not considered. Only a highly simplified approach is used to model downwind sound propagation, although more complex flow fields could be rather easily included in the GFPE methodology. Turbulence scattering and coherence loss are also not considered in the current work. Note that although there is strong progress in computational fluid dynamics modelling, providing detailed flow fields in the case of a ridge mounted wind turbine still remains highly challenging.

2. The Green's Function Parabolic Equation method in undulating terrain

2.1. Basic stepping equation

The two-dimensional stepping equation of the Green's Function Parabolic Equation method is summarized by Eq. (2.1). Some basic features of this technique are discussed below, but a detailed derivation and analysis can be found elsewhere [17, 19, 20]. In this forward propagation approach, the vertical array of pressures p at range $r+dr$ is extrapolated from the previous column at range r.

$$
\begin{aligned}
p(r+dr,z) = \exp(-i \cdot dr \cdot k_0) \cdot \overbrace{\exp(i \cdot dr \cdot (k-k_0))}^{\text{refraction term}} \\
\overbrace{\left\{ \frac{1}{2\pi} \int_{-\infty}^{\infty} \exp\left(i \cdot dr \cdot \sqrt{k_0^2 - k_z^2}\right) \cdot \exp(i \cdot k_z \cdot z) dk_z \int_0^{\infty} \exp(-i \cdot k_z \cdot z') \cdot p(r,z') dz' \right.}^{\text{Direct wave}} \\
\overbrace{+ \frac{1}{2\pi} \int_{-\infty}^{\infty} R(k_z) \cdot \exp\left(i \cdot dr \cdot \sqrt{k_0^2 - k_z^2}\right) \exp(i \cdot k_z \cdot z) dk_z \int_0^{\infty} \exp(i \cdot k_z \cdot z') \cdot p(r,z') dz'}^{\text{Ground-reflected wave}} \\
\overbrace{\left. + 2 \cdot i \cdot \frac{k_0}{Z} \cdot \exp\left(-i \cdot \frac{k_0}{Z} \cdot z\right) \cdot \exp\left(i \cdot dr \cdot \sqrt{k_0^2 - \left(\frac{k_0}{Z}\right)^2}\right) \int_0^{\infty} \exp\left(-i \cdot \frac{k_0}{Z} \cdot z'\right) \cdot p(r,z') dz' \right\}}^{\text{Surface wave}}
\end{aligned}
\quad , (2.1)
$$

with i the imaginary unit, (r,z) the position in respectively the horizontal and vertical direction with dr and dz their spatial discretization steps, Z the ground impedance normalized to that of (unbounded) air ($=\rho c$, with ρ the mass density of air and c the sound speed; local reaction approximation), k_0 the reference wave number (at the ground surface), k the height dependent wave number ($k=2\pi f/c$, with f the sound frequency under consideration), and k_z the wavenumber in the (vertical) spatial (Fourier) domain.

Some distinct contributions in Eq. (2.1) can be identified, namely the direct wave, the ground-reflected wave and a surface wave. Refraction can be efficiently approached by a phase correction due to wave-number variations with height. Temperature (and to a lesser extent humidity) variations with height are directly linked to changes in sound speed [17, 18] involving no approximations. The horizontal components of the wind speed (parallel to the ground) can be approached by an equivalent increase in the sound speed (i.e. the so called "effective sound speed" approach [17, 18]). This step-wise calculation of the acoustic fields allows making both the sound speed profile and the ground parameters range-dependent.

The integrals appearing in the direct and ground-reflected wave terms can be efficiently calculated by relying on the Fourier transform and its inverse, for which numerically very efficient algorithms are commonly available, such as the Fast Fourier Transform (FFT).

In order to represent the wind turbine noise source as a point source, the calculations will rely on the equivalence between (coherent) line source propagation (i.e. the 2D solution) and point source propagation (i.e. the 3D solution) when expressing sound pressure levels relative to free field sound propagation [21] (see Section 4).

2.2. Including terrain undulations

Various approaches for introducing undulating terrain in the PE method can be found, like the general terrain PE (GTPE) [22], the rotated reference frame approach [23, 24, 25] (GFrPE), a stair-step terrain approach using Kirchoff's method [26], and the conformal mapping method [27, 28, 17].

The GTPE can be seen as a generalization of the Crank-Nicholson PE (CNPE) method. This method is applicable to arbitrary terrain profiles and uses terrain-following coordinates. However, analysis has shown that the local slope angles should not exceed roughly 30 degrees [17]. In addition, the CNPE is much less efficient than the GFPE as stepping in the propagation direction needs sub-wavelength discretisation.

The rotated reference frame approach is applicable to the GFPE. The curved ground is treated as a succession of flat zones with different slope angles. The sound field in each domain starts from an array of pressure values, orthogonal to the local slope, as calculated from the previous domain. A number of reduced propagation steps are thus needed near the

interface to accurately construct the next domain's starting field, which can strongly increase computing times [25]. Sudden slope changes along the propagation path are difficult to handle.

The stair-step approach might be attractive due to its simplicity. The terrain profile is reduced to a succession of best-fitting steps that are each treated as small vertical barriers. The part of the sound field covered by each step is then set to zero. This method further needs a vertical coordinate shift to continue propagation from the top of the next step. Combining the foregoing approach with variable step widths provides great flexibility in describing terrain profiles. However, only reflection on horizontal surfaces is modelled. This means that waves reflected obliquely in the direction of sound propagation cannot subsequently interfere along the propagation path. Only part of the acoustic energy will be sent in that direction due to diffraction at step corners, thereby potentially resulting in a significant loss in accuracy.

In this study, the conformal mapping (CM) method will be used, which is a computationally highly efficient approach to account for undulating terrain. The CM method is based on the theoretically perfect analogy between a circularly curved ground surface with radius R_c and a refracting atmosphere with the following exponential sound speed profile c:

$$c = c_0 e^{\frac{z}{R_c}} , (2.3)$$

with $R_c>0$ for concave ground and $R_c<0$ for convex ground, z the height above the ground and c_0 the reference sound speed.

The shielding caused by convex terrain can thus be approached by sound propagating over flat terrain in an upwardly refracting atmosphere, while concave ground is simulated by a downwardly refracting atmosphere. A change in sound speed profile comes at almost no additional computational cost in the PE model. Note that such artificially refracting atmospheres due to ground curvature are typically much stronger than those observed due to real wind flows in the atmospheric boundary layer. The latter, however, can be superimposed on the artificial profile due to ground curving, thus allowing account to be taken of both terrain undulation and atmospheric refraction.

The main limitation here is the need for simplification to circularly curved terrain segments. Care is needed to account for the coordinate transform between the real (curved ground) system and the artificially refractive flat PE domain.

3. Hybrid analytical-CM GFPE model

When applying the GFPE to the specific case of sound propagation across a valley from a ridge mounted wind turbine, two fundamental problems appear.
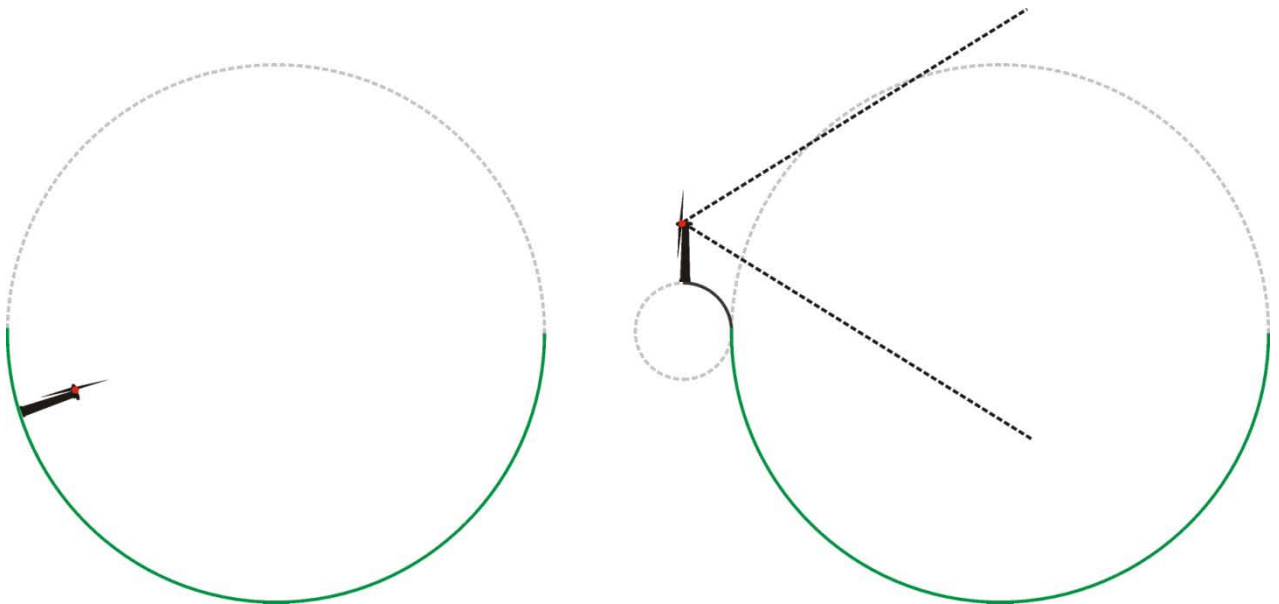

Figure 1. Schematic representation of two fundamental problems associated with CM-GFPE modelling applied to sound propagation from a ridge wind turbine.

Firstly, a direct application of the conformal mapping approach would actually mean that the source becomes oriented perpendicular to the curved ground. Clearly, such a configuration, as schematically illustrated in Fig. (left), deviates strongly from a typical wind turbine case. A more realistic scenario, still consistent with the conformal mapping approach, can be achieved by placing two circular ground segments in series [27][17]. The geometry of interest is thus idealized to sound propagation over a small convex circular segment representing the ridge (with artificial upward refraction), followed by sound propagation over part of a large concave cylinder representing the valley (with artificial downward refraction).

A second fundamental problem when using the Parabolic Equation method for such a case is that sound propagation can only be accurately described in a relative small cone, horizontally centred around the source. In the current context with a source at a large height, a major part of the valley would be artificially put in an acoustic shadow zone (see Fig. 1 on the right), leading to inaccurate results. Although applying a higher-order source approximation could extend the cone with correct predictions [17], at the source side of the valley this problem would still remain.

The solution to this problem is found in the fact that the GFPE method is able to commence from any vertical array of pressures that can be accurately calculated at sub-wavelength spacing. There are actually 3 possibilities. Most commonly used is a Gaussian starter (see e.g. Ref. [17]) as the first column of pressures, representing a monopole source. Accuracy up to larger propagation angles can be achieved by a higher-order approach of the latter (see Ref. [17]). Secondly, another full-wave technique can be used to produce a starting field at close distance from the source (see e.g. [29, 21]). A third option, as done in this work, uses the analytical solution for coherent line source diffraction around an impedance cylinder (with circular cross-section), with the line source parallel to the cylinder axis (summarized in Appendix A).

As a result, the current hybrid analytical-CM-GFPE model does not suffer from angle limitations in the source region. As shown in Fig. 2, sound propagation over exactly one quarter of the cylinder, representing the ridge, is simulated to facilitate the coupling to the valley part. This avoids complicated interpolation at the interface with the valley section. Note that for the valley part, the ground can be further split up in segments with different impedance. The starting field must be characterized on a vertical grid with a (logarithmically) decreasing spacing towards higher positions. This is necessary to comply with the conformal mapping coordinate transform from the curved surface to a grid with a uniform vertical spacing in an (artificially) refracting environment [27, 17].
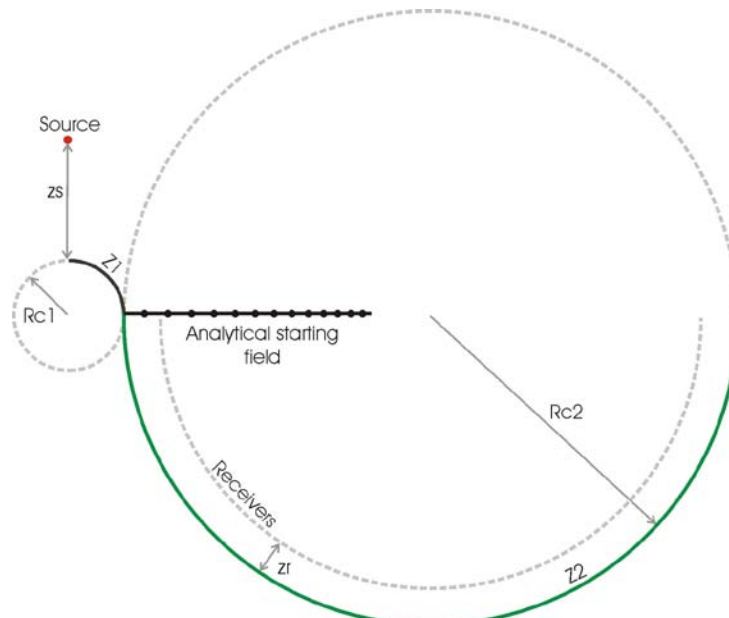

Figure 2: Geometry of the hybrid analytical-CM GFPE model for simulating sound propagation from an elevated sound source, positioned at a ridge (radius R_{c1}, source height z_s), towards a valley (radius R_{c2}, receiver heights z_r). Z_1 and Z_2 are the ground impedances of the ridge and valley part, respectively.

4. Numerical validation

The numerical codes and their parameter choices employed in this study have been validated in two-dimensional cases by inter-comparison with other prediction methods (see Table 1 for an overview). Note that although the numerical

techniques proposed for the hybrid model (see Section 3) are theoretically sound, such an exercise is still useful: it is stressed, for example in Ref. [30], that the GFPE method needs some critical parameter choices, potentially strongly impacting on numerical accuracy. All surfaces were chosen to be rigid, allowing a detailed check of the accuracy of predicted interferences, these becoming most pronounced in such a case. Sound pressure levels relative to free field propagation (unbounded domain) are compared in all cases. This allows focus to be maintained on the physical wave aspects since geometrical divergence, which is always present, is excluded.

In case A, the axi-symmetric [17] CM-GFPE is validated against the analytical solution for sound diffraction around a cylinder (see Appendix A) in case of circularly convex ground. Note that the CM-GFPE could give rise to numerical issues when source and/or receiver heights are large relative to the ground radius [17]. Therefore, a somewhat larger radius was chosen than would otherwise be appropriate for the ridge part of the model.

In case B, the axi-symmetric CM-GFPE is compared to the 2D finite-difference time-domain (FDTD) technique [31] for the case of a circularly concave ground segment. The FDTD technique can be considered as a reference solution over a wide range of acoustical applications. A somewhat larger radius for the ground curvature is now taken compared to validation case A, but still smaller than the radius of a typical valley. This is because the FDTD method is computationally highly demanding. Note that the effect of ground curvature on sound propagation becomes visible at a short distance (see later), thereby justifying this choice. The FDTD code as used here, in its basic form, employs a staircase approach, leading to scattering at the rigid edges of the steps. This effect can be strongly reduced when analysing a lower sound frequency, ensuring a high ratio between wavelength and spatial discretisation step.

In case C, the methodology to develop the GFPE solution from an analytically constructed, coherent line source starting field is compared to the analytical solution of sound propagation over flat rigid ground, directly starting from the source. A two-ray analytical solution for a coherent line source is used for the latter [17, 32, 33].

Table 1. Cross-validation cases considered with indication of their geometries.

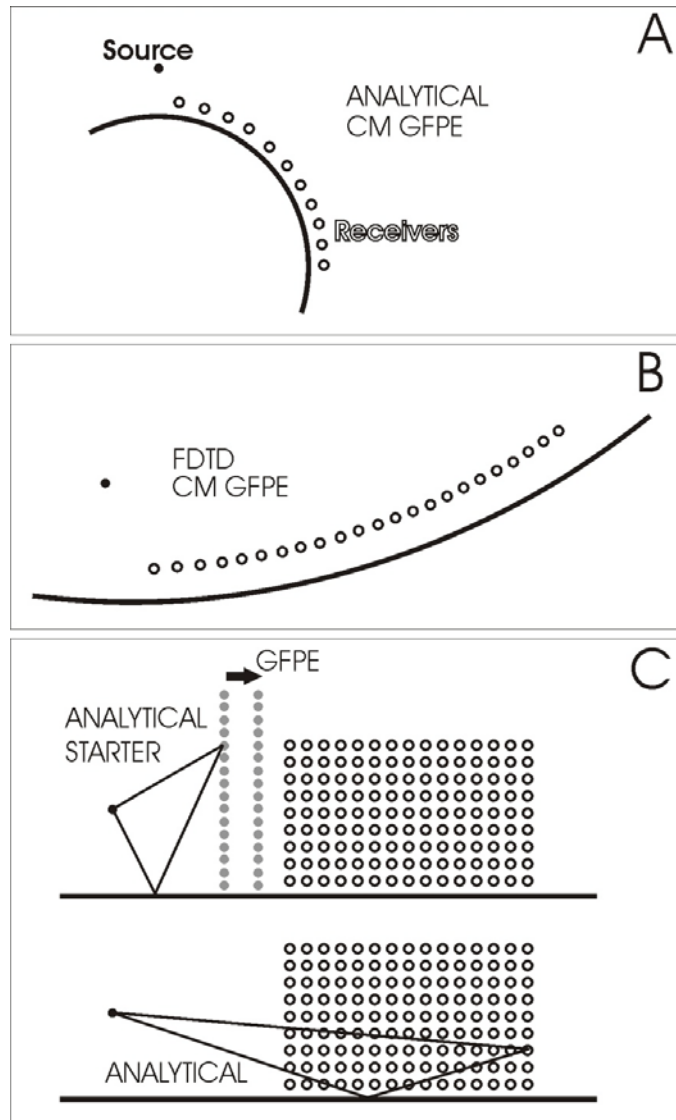| parameter	case A	case B	case C
Models compared	CM-GFPE vs analytical solution	CM-GFPE vs FDTD	GFPE with analytical starter vs (full) analytical solution
Sound frequency (Hz)	500	250	500
R_c (m)	-50 (convex)	100 (concave)	Inf (flat)
z_s (m)	5	5	5
z_r (m)	1	2	
Maximum angle over which propagated	$\pi/2$	$\pi/6$	zone of receivers
Maximum propagation distance along arc (m)	78	50	550

Figure 3. Schematic representation of the validation cases considered.

Validation case A shows good agreement between the analytical solution describing sound propagating around a circular rigid cylinder, and the CM-GFPE. Figure 4 shows the sound field in the transformed coordinate system used by the CM-GFPE (with r the distance along the arc). Receivers are positioned at a fixed height relative to the arc. At close distance, the angle limitation of the PE method becomes visible as discussed before. Note that an 8th order starting field was used here (see Section 3 and Ref. [17]), thereby partly mitigating this inaccuracy. The CM-GFPE yields somewhat less pronounced destructive interference dips that appear at short distance in this particular case; the (very) low levels due to sound wave cancelling are typically not reached with a numerical technique. Near the constructive interferences, differences amount up to 0.6 dB. In the deep shadow zone, some small oscillations in the CM-GFPE could be observed as well.
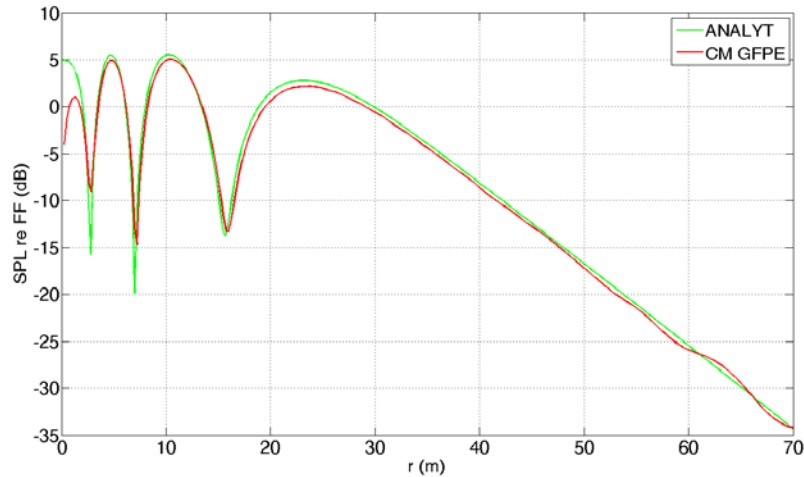
Figure 4. Sound pressure level, relative to free field sound propagation, near a rigid convex circular cylinder at a fixed receiver height along the arc (validation case A).

Fig. 5 shows the comparison between the FDTD and the CM-GFPE methods for a concave rigid surface (validation case B). For comparison, sound propagation in case of the same source-receiver geometry but over flat rigid ground is depicted. The specific curvature of the ground leads to some distinct effects, such as the loss of the strong destructive interference at about 29 m from the source, and the small shifts in interferences at short distance. The agreement between the FDTD and the CM-GFPE methods is very good, with differences smaller than 0.7 dB; similar remarks as for validation case A could be made regarding the angle limitation in PE close to the source, and regarding the magnitude of the destructive interferences. Other (small) differences might come from the fact that the FDTD is a full-wave technique, including backward scattering which is fully neglected in the forward-stepping GFPE approach, the stair-step approach in FDTD, and from the fact that there will be small phase errors that are inherent to the FDTD technique [34]. Validation cases A and B further show the accuracy of the equivalence between a point source and coherent line source solution in such complex geometries when expressing results relative to free field sound propagation (see Section 2.1)
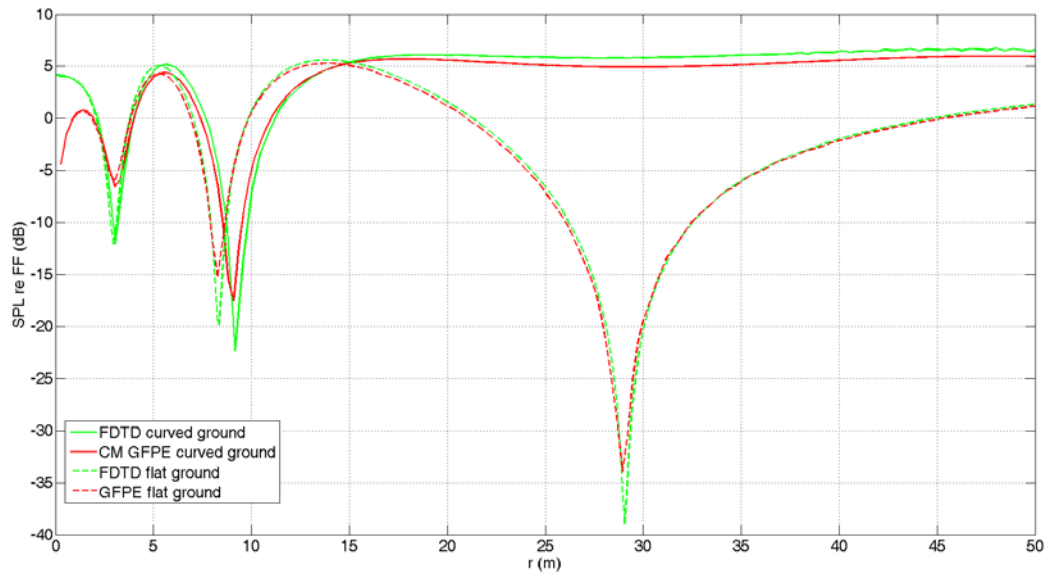

Figure 5. Sound pressure level, relative to free field sound propagation, near a rigid concave circular cylinder at a fixed receiver height ("curved ground", validation case B) along the arc. For comparison, sound propagation over a flat rigid ground with the same source-receiver positioning is depicted as well ("flat ground").

Validation case C (see Fig. 6 and 7) shows excellent agreement between the analytical solution applied to a dense receiver grid, and the analytical starter propagated further with GFPE. The analytical starter is located at 50 m from the source. Only predictions from that distance on are depicted. The field plots presented in Fig. 6 are almost

indistinguishable. The level differences plotted in Fig. 7 show some small deviations only at the zones where the conditions for destructive interference are met.
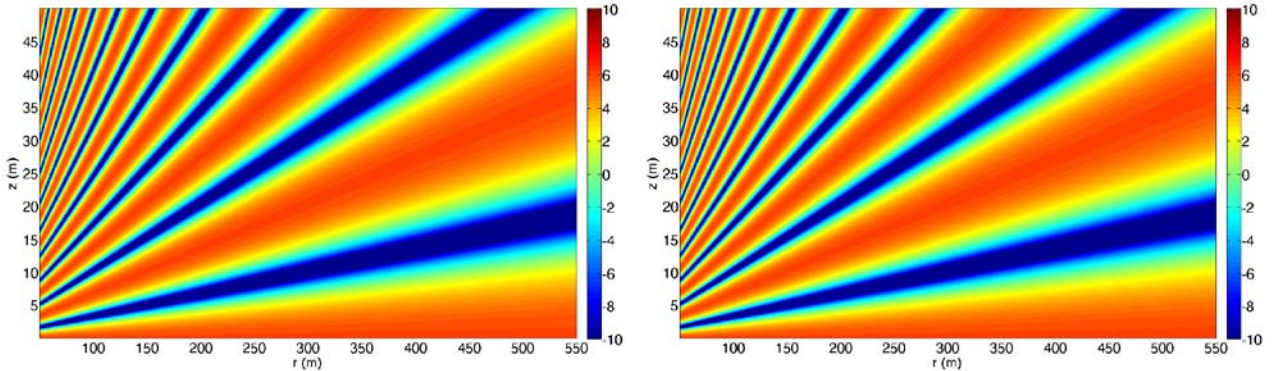

Figure 6. Sound pressure level, relative to free field sound propagation (in dB), over flat rigid ground in a dense receiver grid. On the left, GFPE results using an analytical starting field are depicted, on the right the (full) analytical solution (validation case C).
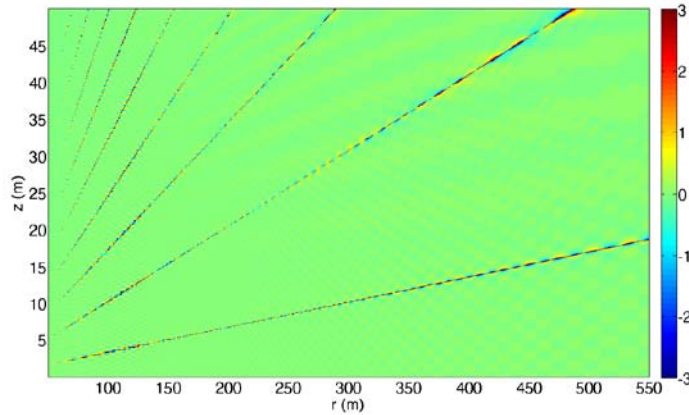

Figure 7. Sound pressure level difference (in dB) between GFPE predictions starting from an analytically constructed starting field and the full analytical solution for sound propagation over flat rigid ground (validation case C).

5. Calculation example: valley ground type

This section shows the potential of the proposed hybrid analytical-CM-GFPE methodology to assess sound pressure levels across a valley in the case of a single ridge wind turbine. The influence of valley ground type is studied.

Sound propagating from a point source (concentrating all the wind turbine's emitted acoustic energy at hub height) at a height z_s=75 m on top of the ridge is considered. The ridge part is rigid and has a radius R_{c1}=10 m. Predictions are made across the adjacent valley with a radius R_{c2} of 500 m at a fixed receiver height z_r=4 m (i.e. the typical receiver height as used in noise mapping). Two valley ground types are modelled, namely rigid and grass-covered ground. For the latter, the common Delany and Bazley impedance model [35] has been used as being appropriate to model reflection from grassland, and characterized by a flow resistivity of 200 kPa s/m^2.

The following numerical parameters were used for the simulations. An absorption layer [17] thickness of 150 wavelengths is chosen with the ratio between *dr* and *dz* being set to 30. These choices are consistent with the guidelines presented in Ref. [26]. In order to sufficiently assess the sound field along the arc, and taking into account the strong (artificial) refraction to represent the ground curvature, 40 computational cells per wavelength were chosen in the vertical direction. As a result, the spatial step *dr* stays below the wavelength. The starting field is constructed in detail up to 75 % of the valley radius. No accuracy loss was observed by reducing the spatial sampling while calculating the starting field to 5 cells per wavelength, followed by linear interpolation. Part of a *Hanning* window was used to gradually allow the pressure to go to zero towards the top of the calculation domain in order to prevent spurious reflections. Analysis is performed in octave bands. Twenty sound frequencies were individually simulated with the hybrid analytical/CM-GFPE model to constitute each band.

Numerical results depicted in Fig. 8 show a rather complex sound pressure level distribution along the valley. In both ground type scenarios, significant shielding is observed directly near the source side of the valley. However, strong differences are predicted further across the valley. Starting from about the centre of the valley, near free field sound propagation is predicted at all octave bands for the rigid ground, while there is a much stronger reduction along the grass-covered valley. Effects become increasingly pronounced with increasing sound frequency, consistent with the fact that surface impedance decreases with frequency. These numerical simulations indicate the importance of ground type in case of ridge wind turbines emitting sound into a valley. This behaviour deviates from wind turbine sound propagation above flat ground, where effects of ground type are typically much less pronounced [36].

An estimation of the total wind turbine received sound pressure level is shown in Fig. 9, for both ground types. A (relative) spectrum is considered to allow balancing the importance of the different octave bands as they behave quite differently during propagation across the valley. To perform this analysis, the mean over a large set of spectral source power level measurements near large horizontal axis wind turbines with a power production of more than 2 MW, as reported in Ref. [15], is used. This spectrum is repeated in Appendix B.

When assuming a total sound power level of 105 dBA, the 35 dBA broadband exposure level (i.e. -70 dBA in Fig. 9) below which negative noise-related effects are not expected (following Ref. [13], see introduction), is predicted after 240 m (28°, relative to the interface between the ridge and valley segment) and 662 m (76°) propagation across the valley, for grass-covered and rigid ground, respectively. Note that these predicted distances involve a single wind turbine only; a series of wind turbines positioned on a ridge would be common practice, however.

Note that in this assessment, the specific noise emission characteristics of wind turbines located on ridges is not included, neither are the complex wind fields that might be expected at such locations. In a strongly simplified approach, a logarithmical wind speed profile (homogeneous atmosphere) is assumed following the valley terrain, using an aerodynamic roughness length of 0.05 m and a friction velocity of 0.4 m/s. Atmospheric absorption [37] is modelled assuming an air temperature of 10 °C, a relative humidity of 70 % and an atmospheric pressure of 101300 Pa. The frequency range considered includes the octave band with centre frequency 2 kHz. For reasons of computational efficiency, the very time consuming sound propagation calculations for the 2 kHz-octave band were not performed (and the 1 kHz band results were recycled). This is justified by the fact that atmospheric absorption becomes pronounced at these higher frequencies and source power levels start to drop; a more accurate assessment of the propagation at this band would therefore only slightly increase accuracy when assessing total noise exposure levels from the wind turbine.
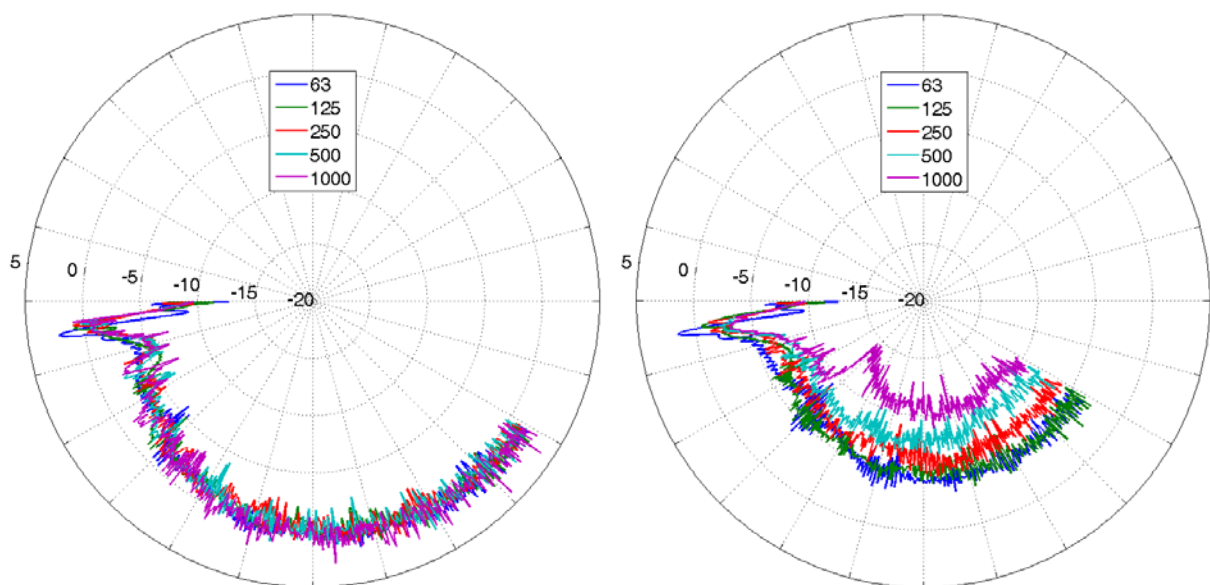

Figure 8: Predicted sound pressure levels (relative to free field sound propagation, in dB) across the valley, in case of a rigid (left) and a grass-covered valley (right), at a receiver height of 4 m. Octave bands with centre frequencies ranging from 63 Hz till 1 kHz are presented.
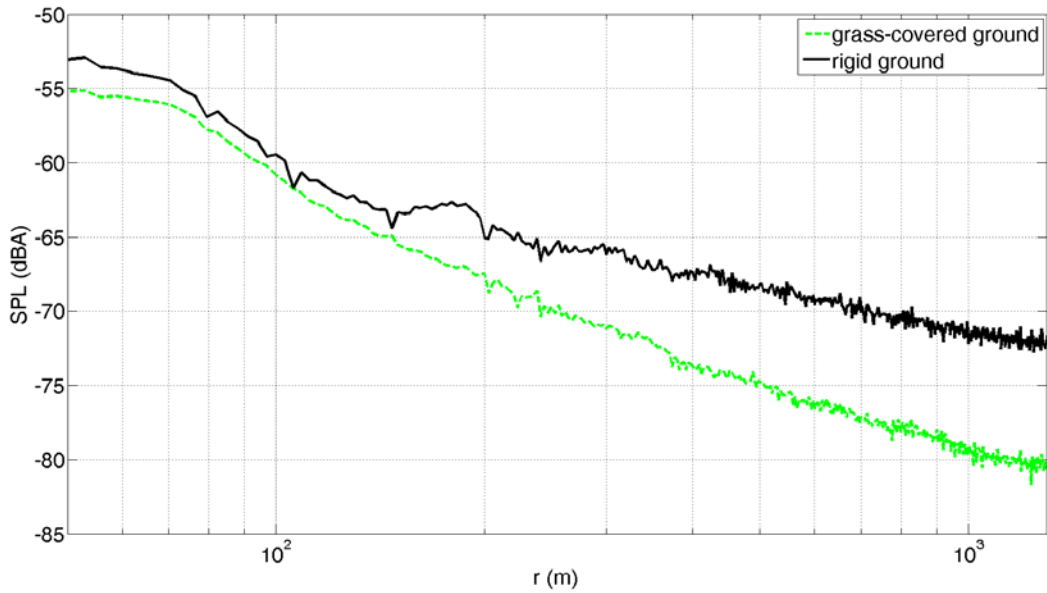
Figure 9: Predicted sound pressure levels at a receiver height of 4 m across the valley arc, in case of rigid and grass-covered valley ground. The total source power level is normalized to 0 dBA (see Appendix B).

6. Conclusions

A hybrid analytical-CM-GFPE methodology is presented to model sound propagation from a ridge mounted wind turbine, represented here by an elevated point source above the ridge, across an adjacent valley. The hybrid method relies on an analytical solution for sound diffraction around an impedance cylinder and the conformal mapping GFPE technique. The geometry is simplified to a convex segment with a small radius, representing the ridge, followed by a large-radius concave circular segment, representing the valley. The hybrid model overcomes issues such as the unrealistic positioning of the source that would otherwise result from the conformal mapping approach, and the general angle limitation of the PE method. Various aspects of the model were successfully validated by means of cross-validations against other numerical or analytical techniques. Calculation examples show the complex sound pressure level distribution in such a ridge-valley geometry. At the source side of the valley, noise shielding from a (single) wind turbine is predicted. Starting from the centre of the valley, near free field sound propagation is observed at all octave bands for the rigid ground case, while there is a strong level reduction along a grass-covered valley. Although wind speed profiles were highly idealized in this work, the calculation methodology has the potential to include the effect of refraction and turbulent scattering as a result of the complex flow fields that might be associated with such a wind turbine placement.

Appendix A : Analytical solution for coherent line source diffraction around an impedance cylinder
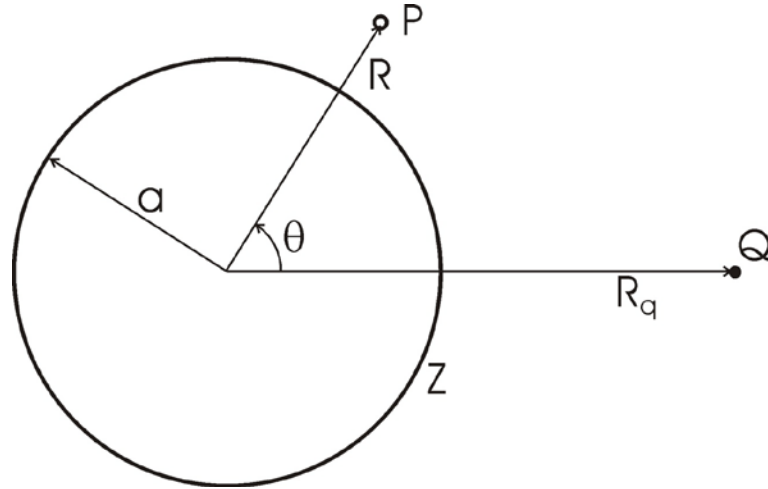

Figure 10: Overview of parameters involved in the analytical solution for coherent line source diffraction around an impedance cylinder.

The total pressure p at point P, at a (radial) distance R relative to the origin of the cylinder, emitted by a coherent line source at point Q, parallel to the cylinder axis and at a distance R_a from the origin of the cylinder, consists of the direct contribution from Q to P ($=p_d$), and the scattered sound pressure ($=p_s$) (see Ref. [33]):

$$p = p_d + p_s . \text{(A.1)}$$

The direct contribution is calculated as follows (assuming a unity-amplitude source):

$$p_d = H_0^2\left(k_0\sqrt{R_q^2 + R^2 - 2\cdot R_q \cdot R \cdot \cos(\theta)}\right). \text{(A.2)}$$

Calculating the scattered field is somewhat more involved, and needs following summation:

$$p_s = \sum_{m=0}^{\infty} a_m \cdot \delta_m \cdot J_m\left(k_0 R_q\right) \cdot H_m^2\left(k_0 R\right) \cdot \cos\left(m\theta\right), \text{(A.3)}$$

with

$$\delta_m = \begin{cases} 1; m = 0 \\ 2; m > 0 \end{cases}. \text{(A.4)}$$

The term a_m in Eq. (A.3) is calculated as follows:

$$a_m = -\frac{i\cdot J_m'\left(k_0 a\right) + \dfrac{1}{Z}\cdot J_m\left(k_0 a\right)}{i\cdot H_m'^2\left(k_0 a\right) + \dfrac{1}{Z}\cdot H_m^2\left(k_0 a\right)} \cdot \frac{H_m^2\left(k_0 R_q\right)}{J_m\left(k_0 R_q\right)}. \text{(A.5)}$$

The derivatives of the Bessel and Hankel functions, with respect to their arguments, can be calculated using the following expressions:

$$J_m'\left(k_0 a\right) = \frac{m}{k_0 a} J_m\left(k_0 a\right) - J_{m+1}\left(k_0 a\right), \text{(A.6)}$$

13

$$H_m'^2(k_0 a) = \frac{1}{2}\left(H_{m-1}^2(k_0 a) - H_{m+1}^2(k_0 a)\right). \text{(A.7)}$$

In the equations above, k_0 is the wave number, a the cylinder radius, θ the angle between source and receiver, H_m^2 the Hankel function of mth order and second kind, J_m the Bessel function of order m, and Z the (normalized) locally reacting surface impedance of the cylinder.

Appendix B : Wind turbine source power spectrum

The source power level spectrum depicted in Fig. 11 was used to calculate total A-weighted exposure levels. This spectrum is the average based on a large number of measurements near horizontal axis wind turbines with a power production of more than 2 MW, as reported by Ref. [15].
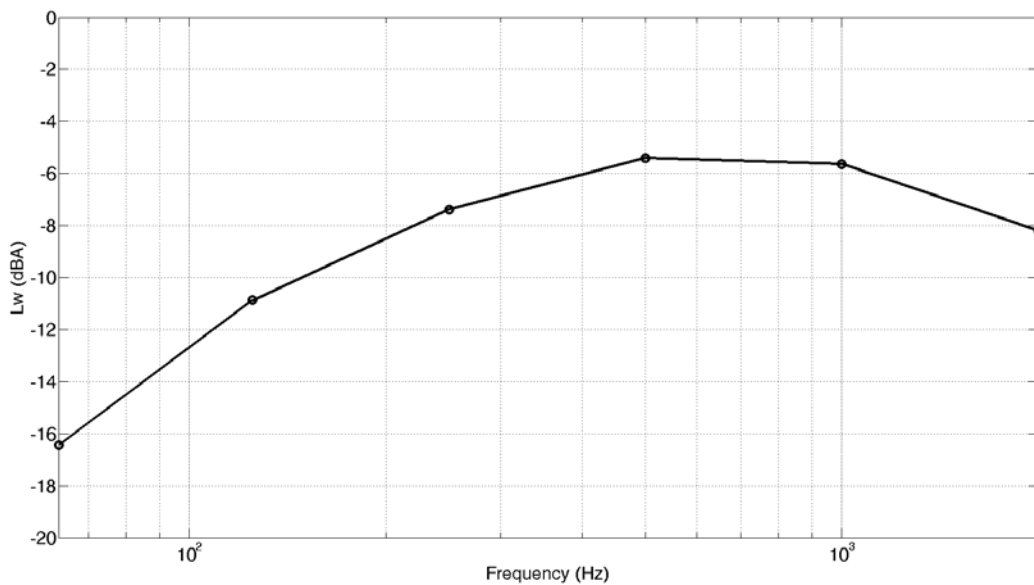

Figure 11. Source power level spectrum used for the calculations depicted in Fig. 9, based on Ref. [15]. The spectrum was normalized to a total source power level of 0 dBA.

References

1. Tabassum-Abbasi, M., Abbasi, T. & Abbasi, S. 2014. Wind energy: Increasing deployment, rising environmental concerns. *Renew Sust Energ Rev* **31**, 270-288.
2. Kim, H., Lee, S., Son, E., Lee, S. & Lee, S. 2012. Aerodynamic noise analysis of large horizontal axis wind turbines considering fluid–structure interaction. *Renew Energ* **42**, 46-53.
3. Pedersen, E. & Waye, K. 2004. Perception and annoyance due to wind turbine noise - a dose-response relationship. *J Acoust Soc Am* **116**, 3460-3470.
4. Pedersen, E. & Waye, K. 2007. Wind turbine noise, annoyance and self-reported health and well-being in different living environments. *Occup Environ Med* **64**, 480-486.
5. Shepherd, D., McBride, D., Welch, D., Dirks, K. & Hill, E. 2011. Evaluating the impact of wind turbine noise on health-related quality of life. *Noise Health* **13**, 333-339.
6. Janssen, S., Vos, H., Eisses, A. & Pedersen, E. 2011. A comparison between exposure-response relationships for wind turbine annoyance and annoyance due to other noise sources. *J Acoust Soc Am* **130**, 3746.
7. Bolin, K., Nilsson, M. & Khan, S. 2010. The Potential of Natural Sounds to Mask Wind Turbine Noise. *Acta Acust united Ac* **96**, 131-137.
8. Van Renterghem, T., Bockstael, A., De Weirt, V. & Botteldooren, D. 2013. Annoyance, detection and recognition of wind turbine noise. *Sci Total Environ* **456-457**, 333-345.
9. Wharton, S., Newman, J., Qualley, G. & Miller, W. 2015. Measuring turbine inflow with vertically-profiling lidar in complex terrain. *J Wind Eng Ind Aerod* **142**, 217–231.

10. Hunt, J., Leibovich, S. & Richards, K. 1988. Turbulent shear flows over low hills. *Q J Roy Meteor Soc* **114**, 1435–1470.
11. Lemelin, R., Surry, D. & Davenport, A. 1988. Simple approximations for wind speed-up over hills. *J Wind Eng Ind Aerod* **28**, 117-127.
12. Lubitz, W. & White, B. 2007. Wind-tunnel and field investigation of the effect of local wind direction on speed-up over hills. *J Wind Eng Ind Aerod* **95**, 639-661.
13. Evans, T. & Cooper, J. 2011. Comparison of predicted and measured wind farm noise levels and implications for assessments of new wind farms. *Proceedings of ACOUSTICS 2011, Gold Coast, Australia.*
14. Schmidt, J. & Klokker, M. 2014. Health Effects Related to Wind Turbine Noise Exposure: A Systematic Review. *PLoS ONE.*
15. Søndergaard, B. 2014. Noise and Low frequency noise from Wind Turbines. *Proceedings of Internoise 2014*, Melbourne, Australia.
16. Keith, S., Feder, K., Voicescu, S., Soukhovtsev, V., Denning, A., Tsang, J., Broner, N., Richarz, W. & van den Berg, F. 2016. Wind turbine sound power measurements. *J Acoust Soc Am* **139**, 1431-1435.
17. Salomons, E. 2001. *Computational atmospheric acoustics.* Kluwer, Dordrecht, The Netherlands.
18. Ostashev, V. & Wilson, D. 2016. *Acoustics in moving inhomogeneous media (second edition).* CRC Press, Boca Raton – London – New York.
19. Gilbert, K. & Di, X. 1993. A fast Green's function method for one-way sound propagation in the atmosphere. *J Acoust Soc Am* **94**, 2343-2352.
20. Salomons, E. 1998. Improved Green's function parabolic equation method for atmospheric sound propagation. *J Acoust Soc Am* **104**, 100–111.
21. Van Renterghem, T., Salomons, E. & Botteldooren, D. 2005. Efficient FDTD-PE model for sound propagation in situations with complex obstacles and wind profiles. *Acta Acust united Ac* **91**, 671–679.
22. Sack, R. & West, M. 1995. A parabolic equation for sound propagation in two dimensions over any smooth terrain profile : the Generalised Terrain Parabolic Equation (GT-PE). *Appl Acoust* **45**, 113-129.
23. Collins, M. 1990. The rotated parabolic equation and sloping ocean bottoms. *J Acoust Soc Am* **87**, 1035-1037.
24. Bérengier, M., Gauvreau, B., Blanc-Benon, P. & Juvé, D. 2003. Outdoor Sound Propagation: A Short Review on Analytical and Numerical Approaches. *Acta Acust united Ac* **89**, 980-991.
25. Van Renterghem, T., Botteldooren, D. & Lercher, P. 2007. Comparison of measurements and predictions of sound propagation in a valley-slope configuration in an inhomogeneous atmosphere. *J Acoust Soc Am* **121**, 2522-2533.
26. Cooper, J. 2003. Parameter selection in the Green's function parabolic equation for outdoor sound propagation over varied terrain. Phd thesis, The Pennsylvania State University, U.S.
27. Di, X. & Gilbert, K. 1994. The effect of turbulence and irregular terrain on outdoor sound propagation. Proceedings of the 6th Symposium on long-range sound propagation, Ottawa, Canada, 315-333.
28. Li, K., Wang, Q. & Attenborough, K. 1998. Sound propagation over convex impedance surfaces. *J Acoust Soc Am* **104**, 2683-2691.
29. Defrance, J., Salomons, E., Noordhoek, I., Heimann, D., Plovsing, B., Watts, G., Jonasson, H., Zhang, X. T., Premat, E., Schmich, I., Aballea, F., Baulac, M. & de Roo, F. 2007. Outdoor sound propagation reference model developed in the European Harmonoise project. *Acta Acust united Ac* **93**, 213-227.
30. Cooper, J. & Swanson, D. 2007. Parameter selection in the Green's function parabolic equation. *Appl Acoust* **68**, 390-402.
31. Botteldooren, D. 1995. Finite-difference time-domain simulation of low-frequency room acoustic problems. *J Acoust Soc Am* **98**, 3302-3308.
32. Attenborough, K., Li, K. & Horoshenkov, K. 2007. *Predicting outdoor sound.* Taylor and Francis, London and New York.
33. Mechel, F. 2008. *Formulas of acoustics (2nd edition).* Springer-Verlag, Berlin-Heidelberg-New York.
34. Van Renterghem, T. & Botteldooren, D. 2007. Prediction-step staggered-in-time FDTD: an efficient numerical scheme to solve the linearised equations of fluid dynamics in outdoor sound propagation. *Appl Acoust* **68**, 201-216.
35. Delany, M. & Bazley, E. 1970. Acoustical properties of fibrous absorbent materials. *Appl Acoust* 3, 105-116.
36. Sims, J., Bullmore, A., Van Renterghem, T. & Horoshenkov, K. Wind turbine noise propagation – results of numerical modelling techniques to investigate specific scenarios. Proceedings of Wind Turbine Noise 2015, Glasgow, UK.
37. ISO 9613-1:1996. *Acoustics – attenuation of sound during propagation outdoors – part 1.* Geneva, Switzerland: International Organisation for Standardisation.